ORIGINAL RESEARCH

American Society of Plant Biologists | SEB SOCIETY FOR EXPERIMENTAL BIOLOGY | WILEY

High spatial resolution imaging of the dynamics of cuticular lipid deposition during Arabidopsis flower development

Liza E. Alexander[1,2] | Jena S. Gilbertson[1] | Bo Xie[1,2] | Zhihong Song[1,2] | Basil J. Nikolau[1,2]

[1]Roy J. Carver Department of Biochemistry, Biophysics and Molecular Biology, Iowa State University, Ames, IA, USA

[2]Center for Metabolic Biology, Iowa State University, Ames, IA, USA

Correspondence
Basil J. Nikolau, Roy J. Carver Department of Biochemistry, Biophysics and Molecular Biology, Iowa State University, Ames, IA 50011, USA.
Email: dimmas@iastate.edu

Present address
Jena S. Gilbertson, Illinois College of Optometry, Chicago, IL, 60616, USA
Bo Xie, Office of Intellectual Property and Technology Transfer, Economic Development Core Facility, Iowa State University, Ames, IA, 50010, USA
Zhihong Song, Office of Pharmaceutical Quality, Center for Drug Evaluation and Research, U.S. Food and Drug Administration, Silver Spring, MD, 20993, USA

Abstract

The extensive collection of *glossy* (*gl*) and *eceriferum* (*cer*) mutants of maize and Arabidopsis have proven invaluable in dissecting the branched metabolic pathways that support cuticular lipid deposition. This bifurcated pathway integrates a fatty acid elongation-decarbonylative branch and a fatty acid elongation-reductive branch, which collectively has the capacity to generate hundreds of cuticular lipid metabolites. In this study, a combined transgenic and biochemical strategy was implemented to explore and compare the physiological function of three homologous genes, *Gl2*, *Gl2-like*, and *CER2*, in the context of this branched pathway. These biochemical characterizations integrated new extraction chromatographic procedures with high spatial resolution mass spectrometric imaging methods to profile the cuticular lipids on developing floral tissues transgenically expressing these transgenes in wild-type or *cer2* mutant lines of Arabidopsis. Collectively, these datasets establish that both the maize *Gl2* and *Gl2-like* genes are functional homologs of the Arabidopsis *CER2* gene. In addition, the dynamic distribution of cuticular lipid deposition follows distinct floral organ localization patterns indicating that the fatty acid elongation-decarbonylative branch of the pathway is differentially localized from the fatty acid elongation-reductive branch of the pathway.

1 | INTRODUCTION

The multicellular nature of plants has provided challenges to deciphering the genetic and biochemical mechanisms that regulate extracellular cuticular lipid biogenesis. These lipids are produced by the epidermal cell layer that accounts for only about 10% of the cellular population of the aerial organs of plants (Jellings & Leech, 1982).

Additionally, this biological process is physically distributed among different compartments at the cellular and subcellular levels (plastids, cytoplasm, endoplasmic reticulum, and plasma membrane of epidermal cells). The barriers associated with this complexity have been partially overcome with forward genetic approaches that use *eceriferum* (*cer*) mutants of Arabidopsis (Koornneef et al., 1989), *glossy* (*gl*) mutants of maize (Schnable et al., 1994) and tomato

(Leide et al., 2007; Vogg et al., 2004), and *wax crystal-sparse leaf* (*wsl*) mutants of rice (Wang et al., 2017; Yu et al., 2008), which has led to the molecular identification and characterization of genes involved in cuticle deposition. Many examples indicate, however, that the isolation of the causative gene that gives rise to the defect in cuticular lipid deposition is only the starting point for detailed understanding of the functionality of the isolated gene in the context of cuticle biosynthesis (Bernard & Joubès, 2013; Post-Beittenmiller, 1996; Samuels et al., 2008).

These complexities can be partially overcome by applying detailed proteomic and/or metabolomics characterizations, comparing mutant and wild-type plants. However, a particular limitation with these experiments is the fact that these techniques are generally performed on tissue extracts that homogenize tissues and cells that are at different developmental stages, and thereby losing in situ localization and developmental states of the cell population. Technologies that make use of "reporter" interactions can visualize gene expression at high spatial scale resolution; for example, in situ nucleic acid hybridization and antibody reactivity (Griffin et al., 1998; Küpper et al., 2007; McFadden, 1995), or genetic fusion with fluorescent reporters (Chalfie et al., 1994; Gallagher, 1992; Koo et al., 2007; Ow et al., 1986). Thus, these technologies produce data concerning the spatial distribution of macromolecules and generate data that provide indirect insights of the in vivo flow of intermediates of metabolism through metabolic networks in and among different cells. Moreover, data generated by these techniques are not necessarily dynamic. This gap in the biochemical characterization pertaining to the nature and regulation of metabolism can be partially overcome with mass spectrometric imaging (MSI; McDonnell & Heeren, 2007).

MSI is a rapidly growing technology known for its ability to provide high spatial resolution data on the cellular location of metabolites, detecting extremely small amounts of metabolites (i.e., high sensitivity), and providing chemical identification data concerning the detected analyte. Additionally, among the several molecular ionization techniques that are used in MSI, the use of diverse ionization technologies as in the case of matrix-assisted laser desorption ionization (MALDI)-MSI further enhances the abilities of this technology. Hence, it is now possible to analyze the spatial distribution of a variety of different classes of compounds (e.g., lipids, proteins, and small molecules) in both plant and animal tissues (Amstalden van Hove et al., 2011; Angel & Caprioli, 2013; Jungmann & Heeren, 2012; Lee et al., 2012; Svatoš, 2010).

As exemplary application of this imaging technology, the focus of this study was the characterization of two homologous maize genes, *Gl2* and *Gl2-like*, whose specific biochemical functions are still unclear, but both genes are known to impact cuticular lipid deposition (Alexander et al., 2020; Bianchi, 1975; Tacke et al., 1995). *Gl2* was initially identified as a product of a forward genetic screen (Hayes and Brewbaker, 1928) and, subsequently, following its molecular characterization (Tacke et al., 1995) it led to the identification of the homologous *Gl2-like* gene (Alexander et al., 2020). Similar to *Gl2*, the *CER2* gene was initially characterized as a mutant that affects the normal accumulation of cuticular lipids on Arabidopsis stems

(Jenks et al., 1995; Koornneef et al., 1989; McNevin et al., 1991), and subsequent molecular characterization of this locus established the sequence homology between *GL2* and *CER2* (Negruk et al., 1996; Xia et al., 1996); and these two genes proved to encode archetypal members of the BAHD family proteins (D'Auria, 2006). Additional molecular and genetic analysis identified that the Arabidopsis genome contains four additional *CER2* homologs, these being called *CER2-like* genes (Haslam et al., 2017), one of which had originally been genetically characterized as the *cer26* mutant (Pascal et al., 2013). More recently we compared the functionality of the *Gl2* and *Gl2-like* genes by genetic complementation assays, relative to the function of the Arabidopsis *CER2* gene (Alexander et al., 2020).

In this study we illustrate the application of two specific analytical capabilities that overcome shortcomings associated with traditional "bulk" tissue characterizations. Moreover, many such reported studies of cuticular lipid mutants are limited to assays that measure metabolic outcomes taken at a single time point, and thus ignore the dynamics of the system. Furthermore, the use of more assiduous analytical technologies enabled the detection and measurement of cuticular lipid accumulation patterns in discreet tissue samples. Specifically, we used the on-column large volume injection capabilities of the LVI-PTV injector (Engewald et al., 1999; Wilson et al., 2000) that concentrates dilute samples during the gas chromatography (GC)-injection process, and thus assayed the dynamics of cuticular lipid accumulation during the development of single Arabidopsis flowers. We coupled this capability with the use of MALDI-MSI (Cha et al., 2009; Feenstra et al., 2017; Jun et al., 2010; Lee et al., 2012) to examine the changes in the distribution of cuticular lipids on developing Arabidopsis wild-type and *cer2* mutant flower surfaces, and obtained dynamic cuticular lipid data, at spatial resolution of a few cells.

2 | MATERIAL AND METHODS

2.1 | Plant material and growth conditions

Arabidopsis genetic seed stocks were obtained from the Arabidopsis Biological Resource Center (www.arabidopsis.org). These included seeds of the wild-type Col-0 ecotype, and the SALK_084443C mutant line, which carried a T-DNA insertion mutation at the At4g24510 locus in the Col-0 background, that is, the *cer2-5* mutant allele. As previously described (Alexander et al., 2020), both these Arabidopsis lines used as hosts for transgenes that overexpressed the maize *Gl2* (GRMZM2G098239; Zm00001d002353) or *Gl2-like* (GRMZM2G315767; Zm00001d024317) ORFs. In addition, we generated a control transgenic line that overexpressed the *CER2* ORF in the *cer2-5* mutant background. The expression of all transgenes was under the transcriptional control of the CaMV 35S promoter. All plants were grown in a growth room maintained at 22°C, and under continuous illumination.

Biochemical analyses were conducted on Arabidopsis developing flowers (Figure 1) harvested at four defined stages of

FIGURE 1 Arabidopsis flower development. Stage A are flowers with closed buds; Stage B flowers are identified by the first emergence of petals from the bud; Stage C, the emerging petals are perpendicular to the flower axis; and at Stage D the flower recloses and the developing silique begins to emerge

development: a) Stage A are flowers with closed buds; b) Stage B flowers were identified by the first emergence of petals from the bud; c) Stage C flowers were identified as presenting emerging petals that are perpendicular to the flower axis; and d) Stage D flower reclosed and the developing silique was just starting to emerge. Time-lapse video-photography was used to determine the timing of the transitions between each stage of flower development, and weight of flowers was determined at each of the four development stages, from 2 to 3 biological replicates consisting of 6 to 13 pooled flowers.

2.2 | Cuticular lipid analysis of single Arabidopsis flowers

Extracellular cuticular lipids were extracted from individual flowers at each developmental stage (Stages A to D). Biologically replicated data were gathered by extracting extracellular cuticular lipids from six individual flowers at each stage of development, with each flower being harvested from independent plants. For quantification purposes, an aliquot of 0.01 µg hexacosane, dissolved in chloroform, was applied to the individual flowers, and after the solvent had evaporated, the flowers were immersed in 0.5-mL chloroform for 60 s. After the flower had been removed, the chloroform solvent containing the extracted extracellular cuticular lipids was dried under a stream of N_2 gas. The dried extract was treated with 0.07-mL N,O-Bis (trimethylsilyl) trifluoroacetamide (BSTFA) with 1% trimethyl-chlorosilane (TMCS; Sigma-Aldrich) 70°C for 30 min, and 10 µl was injected into the GC.

GC-MS analysis was performed with an Agilent 6890 GC interfaced to a 5973 mass spectrometer. The GC was equipped with a LVI-PTV inlet injector (Agilent Technologies, Santa Clara, CA), which enabled the analysis of dilute samples by providing a means of concentrating large injection volumes (10-µl). The GC was equipped with a HP-5 ms column (30 m x 0.25 mm i.d. coated with a 0.25 µm film, Agilent Technologies). Chromatography was conducted with a mobile gas phase of helium at a flow rate of 0.1 ml/min. The column oven temperature was programmed to increase from 80°C to 180°C at 20°C/min, and held at this temperature for 1 min, then ramped to 220°C at a rate of 5°C/min, held at this temperature for 5 min, and finally ramped to 320°C at 10°C/min, and held there for 10 min. The interface temperature to the mass spectrometer was at 280°C, and the ionization voltage for mass spectrometry was set at 70 eV.

The GC/MS data files were deconvoluted by National Institute of Standard and Technology Automated Mass spectral Deconvoluted and Identification System (NIST AMDIS) software, and searched against an in-house compound library as well as the NIST 14 Mass Spectral Library. The abundance of the extracellular lipids was calculated based on the peak size of the spiked hexacosane standard.

2.3 | Mass spectrometric imaging of flowers

Flowers collected at the four developmental stages were attached to Indium Tin Oxide (ITO)-coated glass slides (Fisher Scientific, Pittsburg, PA) with double-sided tape. Flowers were carefully opened for imaging the adaxial surfaces of the floral organs using fine tweezers and a dissecting needle. For the abaxial (lower) surface, petals and sepals were carefully dissected and placed on the double-sided tape. Care was taken to ensure that all flower organs were flat on the MS imaging slide. The attached samples are dried in a glass vacuum desiccator for 30–60 min. Flowers were then sputter coated with silver target 3NS (99.95% purity; ESPI Metals, Ashland, OR) for 50 s, using a Cressington 308R Sputter Coater (Redding, CA, USA) at an argon partial pressure of 0.02 mbar, and a current of 80 mA.

A 7T SolariX Fourier Transform Mass Spectrometer (FTICR-MS; BrukerDaltonics) equipped with an MALDI ion source was used for MSI. The spectrometer used a SmartBeam™ II laser with a spot size of 80 μm diameter. All spectra were acquired in positive ion mode, integrating 200 laser shots per image pixel. The laser power was set to 25% with a frequency of 1,000 Hz. The mass scanning range was set from m/z 300 to m/z 800, time of flight value was 0.7 s, and ion cooling time was set to 0.01 s. The mass spectrometer was externally calibrated prior to sample analysis, using arginine standard mixture (Sigma-Aldrich). Images were processed using FlexImaging 4.0 software (BrukerDaltonics). Chemical identification of ions was performed based on theoretical monoisotopic masses of each surface lipid species and the mass tolerance was set to 2 ppm.

3 | RESULTS

3.1 | Developing flowers as an informative system on the dynamics of extracellular cuticular lipid deposition

The relatively rapid rate of tissue differentiation and development that occurs during the emergence of Arabidopsis flowers provides a convenient system to explore the dynamics of extracellular cuticular lipid accumulation. In addition, by using the LVI-PTV injector capabilities (Engewald et al., 1999; Wilson et al., 1997) to concentrate dilute samples during the GC-injection process, we characterized the extracellular cuticular lipid profiles extracted from individual flowers, collected at different stages of flower development. These attributes enabled the dynamic comparison of the cuticular lipid accumulation during flower development of wild-type and cer2-5 mutant plants, and the effect of genetically complementing this mutation by the transgenic expression of a wild-type CER2 allele.

The developmental stages of flowers were defined from their morphological appearances, as follows (Figure 1): Stage A, are flowers with closed buds; Stage B flowers are identified by the first emergence of petals from the bud; at Stage C the emerging petals are perpendicular to the flower axis; and at Stage D the flower recloses and the developing silique begins to emerge. Time lapse videos of two to four replicate flowers enabled the timing of these four stages, relative to Stage A, which was assigned the zero time point. Thus, flowers on wild-type plants reached Stage B at 2.10 ± 0.05 hr, Stage C occurred at 9.50 ± 0.96 hr, and Stage D occurred at 33.5 ± 2.6 hr. Statistical analysis of these data shows that the B to C transition is slowed by the cer2-5 mutation, but this delay is alleviated by the transgenic expression of CER2 in this mutant (Figure 2; Table S1). In parallel, we determined the biomass of these flowers as a quantitative measure of flower growth (Figure 3; Table S2). Thus, although the cer2-5 mutation affects the developmental timing of the flower, it does not alter the biomass of the resulting flowers (Figure 3).

Analysis of the extracellular cuticular lipid load on these developing flowers reveals dynamic changes in the accumulation of the alkyl metabolites. Similar to prior studies of the cuticular
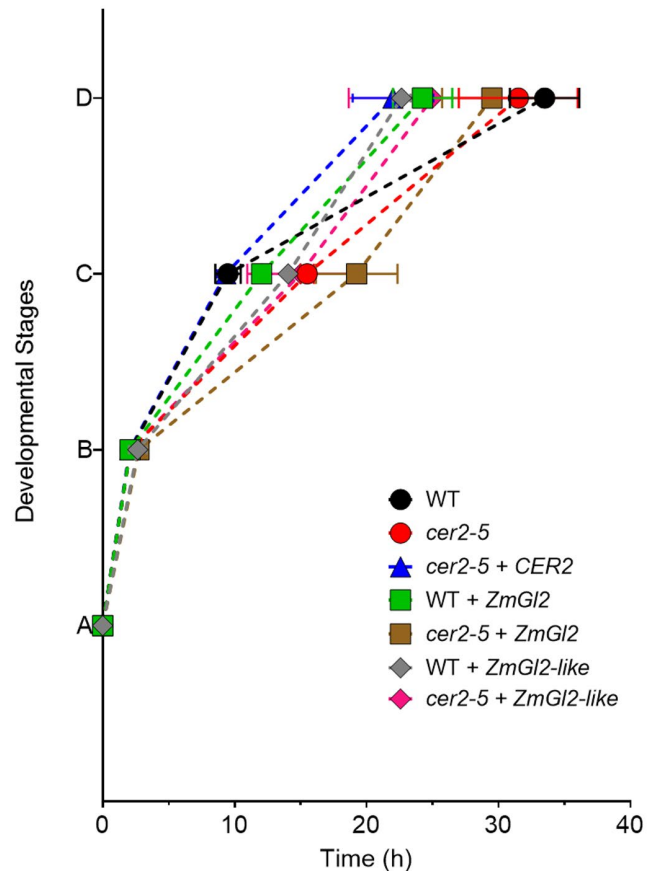

FIGURE 2 Timing of Arabidopsis flower development. Timing of transitions from Stage A to Stages, B, C, and D of nontransgenic and transgenic wild-type and cer2-5 mutant flowers expressing either the CER2 gene or the maize Gl2 or Gl2-like genes. The data are the average of 2–4 replicates ± standard error, determined from time-lapse videos. Statistical evaluation of the significance of the differences among the genotypes was evaluated by Student's t-test (see Table S1)

lipids of Arabidopsis leaves and stems (Hannoufa et al., 1993; Jenks et al., 1995; Koornneef et al., 1989), these metabolites are fatty acids and derivatives, such as primary alcohols, alkanes (linear and iso-branched), ketones, and secondary alcohols (Data Sheet S1), with the latter three metabolite classes being predominant. The accumulation of these lipids increases asymptotically with development, through an initial rapid rate of accumulation (i.e., the transition from Stages A to B) that is as high as 26.3 nmol of lipid/hr/g of fresh weight, which slows to a rate of 1.5–2.6 nmol of lipid/hr/g of fresh weight between Stages C and D (Figures S1 and S2; Tables S3 and S4). The effect of the cer2-5 mutation is to nearly eliminate the initial burst in cuticular lipid accumulation and to reduce the later accumulation rate to near zero (Figures S1 and S2; Tables S3 and S4). As would be expected, the transgenic expression of CER2 in the cer2-5 mutant increases the rate of floral cuticular lipid accumulation to that found with wild-type flowers.

In the context of these genetic-based changes in the dynamics of the total cuticular lipid loads on the flowers, the major components
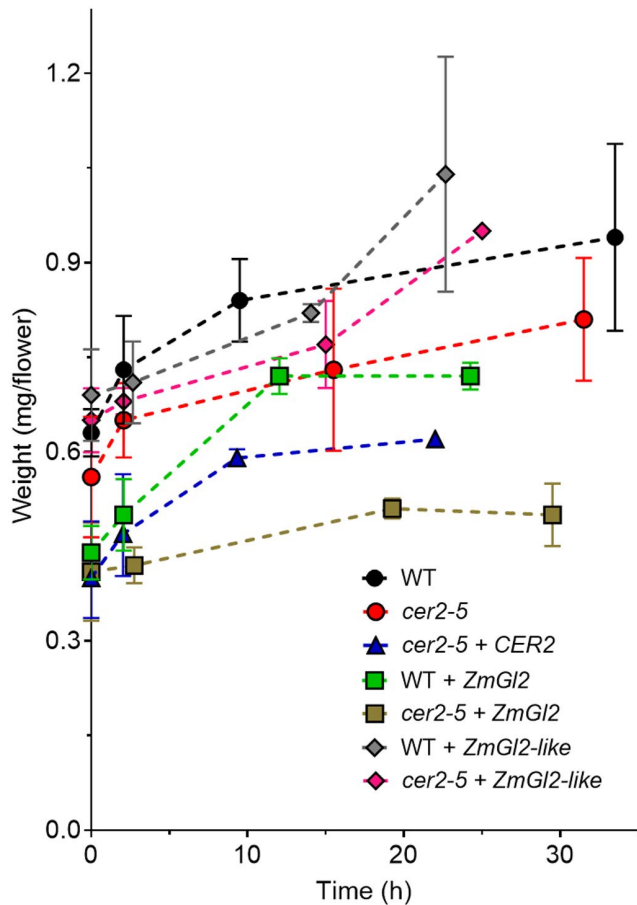
FIGURE 3 Change in biomass with flower development. Fresh weight of flowers ± standard deviation is plotted against time taken for Arabidopsis flowers to reach different stages of development. The fresh weight of 6–13 pooled flowers of the indicated genotypes was weighed at each of the 4 stages of flower development, defined in Figures 1 and 2. The data are the average of 2–3 determinations ± standard deviation. Statistical evaluation of significance of the differences among the genotypes was evaluated by Student's *t*-test (see Table S2)

are always hydrocarbons, which account for 70 to 80% of the quantified cuticular lipids (Figures 4-6; Data Sheet S1). In the wild-type state, over 70%–80% of the hydrocarbons are of 29-carbon chain length, with lesser amounts of other linear chains (25, 27, or 31 carbon atoms) or 2-methyl-branched chains (26, 28, 29, or 30 carbon atoms). The other less abundant classes of cuticular lipids, in descending order of abundance, are secondary alcohols, ketones, primary alcohols, and fatty acids. The dynamic accumulation patterns of the majority of the individual metabolites follow a similar asymptotic curve as the total cuticular lipid accumulation pattern (Figures 4-6). Moreover, with the exception of the VLCFAs, the most abundant chain length of each of these alkyl derivatives match those of the hydrocarbons (i.e., either the same number of carbon atoms or one carbon atom longer than the hydrocarbon), as would be predicted from the currently accepted model of cuticular lipid biosynthesis pathway, that is, VLCFA elongation coupled to either a reductive or decarbonylative branched pathway

(Bianchi et al., 1985; Post-Beittenmiller, 1996). The one exception is the chain-length distribution of the VLCFAs, which are dominated by 20 to 24 carbon chain length, whereas the other alkyl classes are dominated by the longer chain lengths (28–30 carbon atoms).

Tables S3 and S4 tabulate the rates of accumulation for each of the cuticular lipid metabolites between each of the four flower developmental transitions. While the asymptotic rates of accumulation are maintained for most individual components, in the *cer2-5* mutation at the initial stages of development (Stage A-B transition) these rates are approximately ½ the rate determined in the wild-type plants. Two exceptions to this generalization are the net accumulation rates of 26:0 and 28:0 fatty acids and primary alcohols of these chain lengths. The initial rate of accumulation of these metabolites is increased in the *cer2-5* mutant by 2- to 5-fold as compared to the wild type, and this increase is reversed by the transgenic expression of *CER2* (Figure 4; Table S4).

3.2 | Transgenic expression of the maize *Gl2* and *Gl2-like* in the *cer2* mutant restores cuticular lipid accumulation on developing flowers

Using the above data as a baseline, two independent transgenic experiments were conducted to characterize the effect of expressing either the maize GL2 or GL2-like proteins in a wild-type or *cer2-5* mutant background. The expression of either *Gl2* or *Gl2 like* in the *cer2-5* mutant does not affect the developmental timing of the flowers, however, in the wild-type background both transgenes induce a faster rate of flower development (Figure 2 and Table S1). Additionally, the transgenic expression of *Gl2* in both of these genetic backgrounds reduced the mass of the flowers (Figure 3, and Table S2), whereas the *Gl2-like* transgene did not impact the mass of the resulting flowers (Figure 3, and Table S2).

The transgenic expression of either *Gl2* or *Gl2-like* in the *cer2-5* mutant affected an increase in the level of cuticular lipid accumulation on developing flowers. The *Gl2* transgene appears to be more effective in returning the accumulation of cuticular lipids to wild-type levels (Figure S1), whereas the *Gl2-like* transgene only partially rescued this trait (Figure S2). This latter effect is particularly noticeable in the accumulation pattern of the major components, the alkanes, ketones, and secondary alcohols (Figure 6). Thus, whereas the transgenic expression of *Gl2* in the *cer2-5* mutant restores the levels of these lipids to wild-type levels, the transgenic expression of *Gl2-like* in this mutant leads to the accumulation of these lipids at only 50% of the levels found in the wild type (Figures 5 and 6).

3.3 | Nonuniform tissue and cellular-level spatial distribution of epicuticular surface lipids on the abaxial and adaxial surfaces of Arabidopsis flowers

The extraction-based data presented in Figures 4-6 and Figures S1 and S2, integrate the cuticular lipid compositional changes that occur
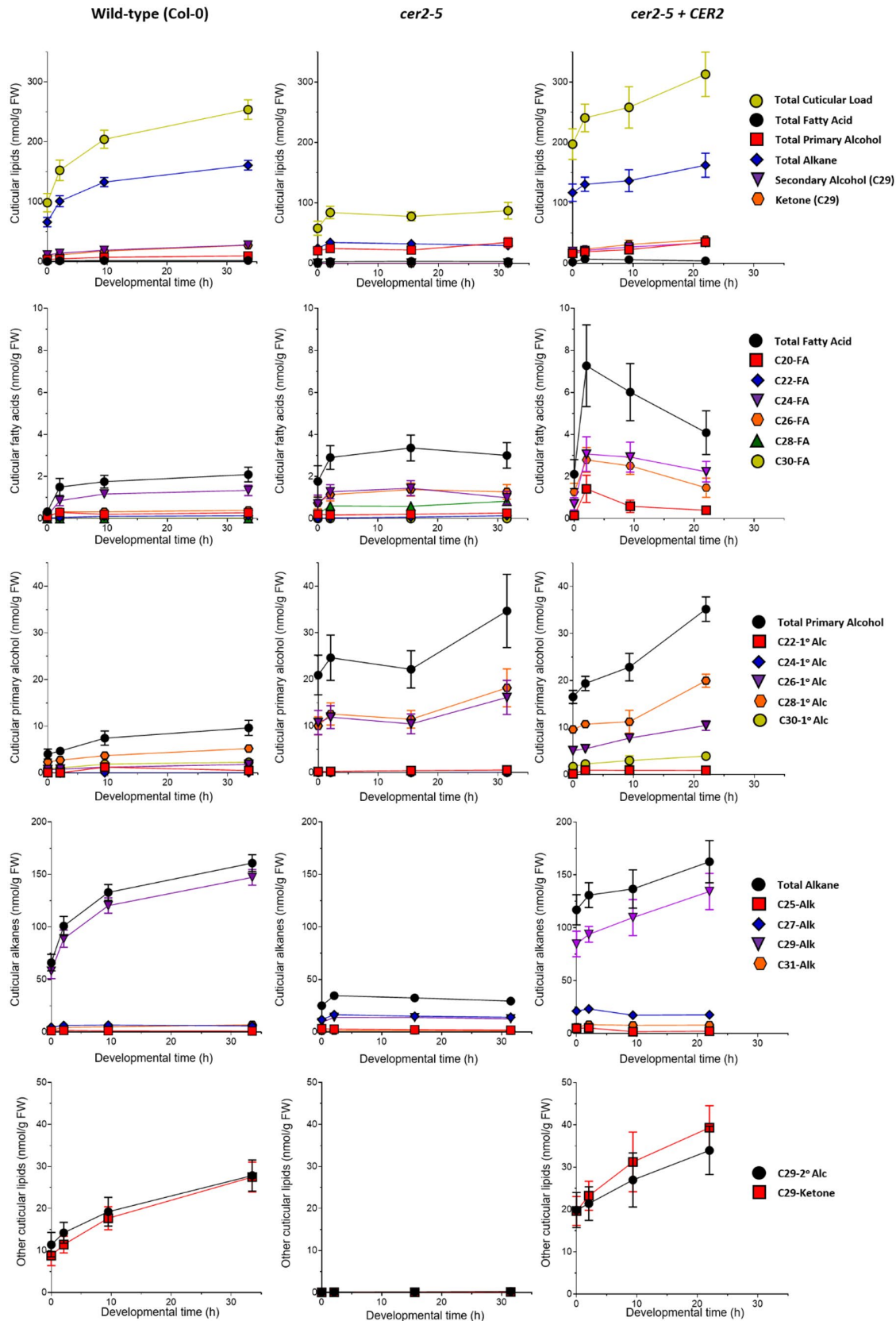
FIGURE 4 Cuticular lipid accumulation on developing Arabidopsis flowers. Cuticular lipids were extracted from individual Arabidopsis flowers of wild-type, *cer2-5* mutant, and *CER2* overexpressed in the mutant, and analyzed using a GC equipped with a LVI-PTV inlet injector (see Materials and Methods). The data represent the average ± standard error of two independent experiments for the wild-type and *cer2-5* mutant arranged in order of most abundant metabolites
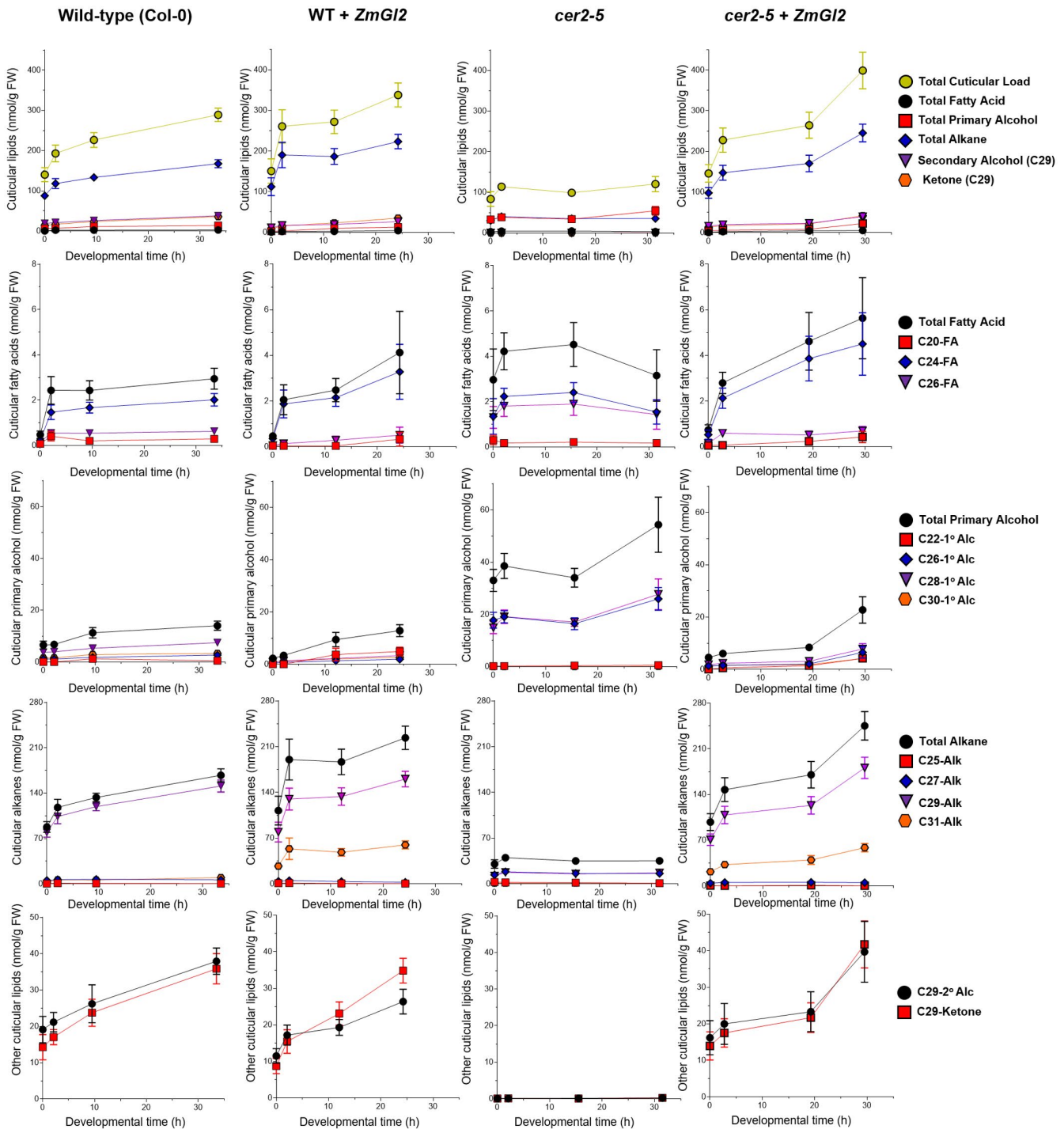
FIGURE 5 Cuticularlipid accumulation on developing Arabidopsis flowers. Cuticular lipids were extracted from individual flowers of genotypes: wild-type (Col-0), *cer2-5* mutant, and either of these lines expressing maize *Gl2* transgene. The data represent average ± standard error of six replicates arranged in order of highest abundance

on a number of different flower tissues (e.g., petals, sepals, anthers, and stigmatic tissues), each of which is on a different developmental schedule (Alvarez-buylla et al., 2010; Smyth, 1990). Therefore, we applied in situ mass spectrometric imaging, specifically MALDI-MSI technology (Dong et al., 2016; Lee et al., 2012; Kaspar et al., 2011), to individually localize these metabolites at a high spatial scale (~80 μm), which enables the visualization of the accumulation

of these metabolites among the different tissues of the flower. Given that Arabidopsis epidermal cells present surface areas that are ~1,000 to 4,000 μm^2 (Cookson et al., 2006; Kheibarshekan Asl et al., 2011; Robinson et al., 2018), and the laser spot size used in the MSI experiments has diameter of ~80 μm (i.e., 5,000 μm^2 area), we estimate that these MSI data are visualizing the surface distribution of cuticular lipids at a resolution as small as 2–4 cells. Moreover,
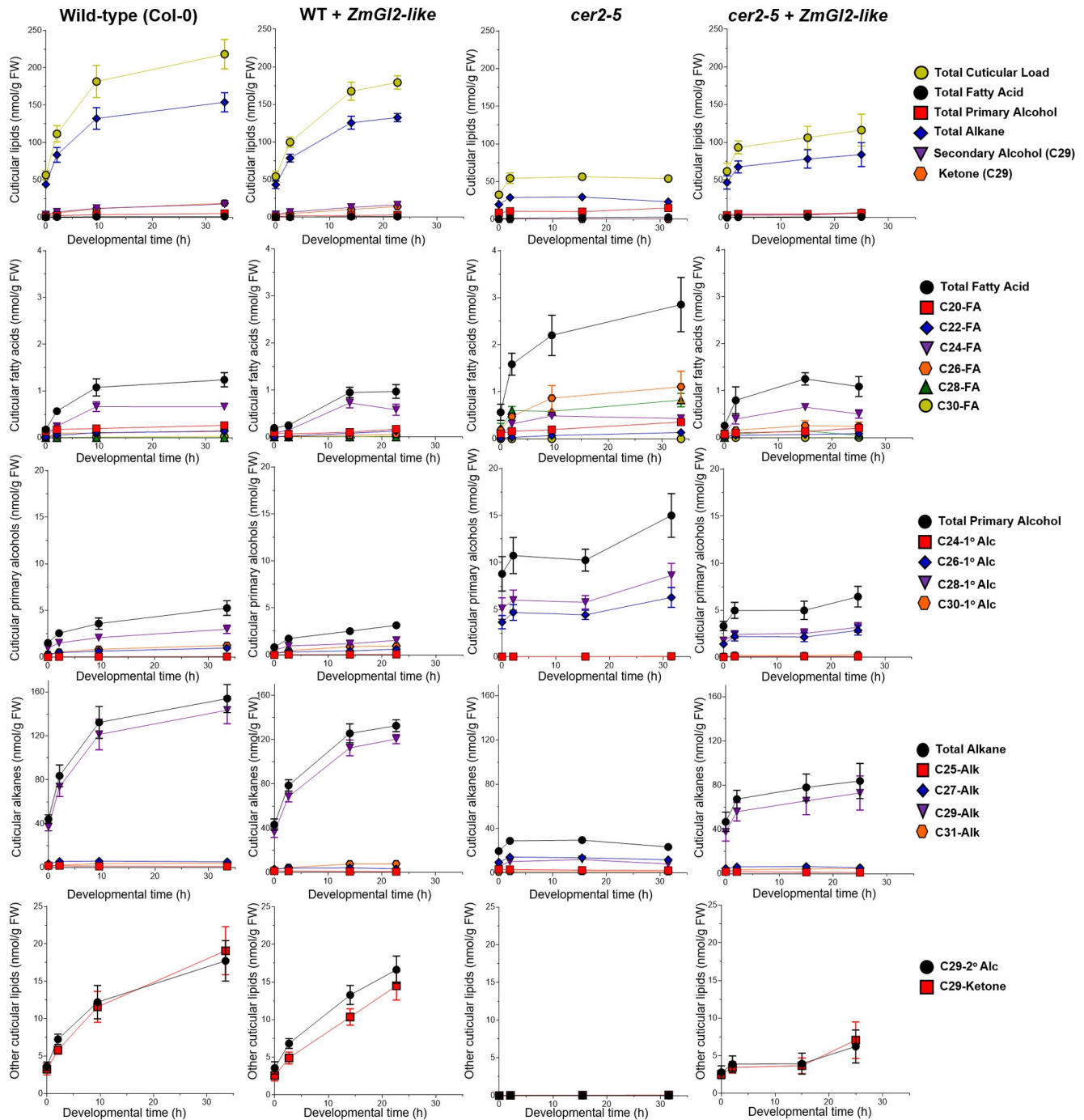
FIGURE 6 Cuticular lipid accumulation on developing Arabidopsis flowers. Cuticular lipids were extracted from individual flowers of genotypes: wild-type (Col-0), *cer2-5* mutant, and either of these lines expressing maize *Gl2-like* transgene. The data represent average ± standard error of six replicates arranged in order of highest abundance

MALDI-MSI was used to investigate the cuticular surface lipid distribution on both surfaces of the developing flowers (Figure 7a), which enabled the comparison of the distribution of individual metabolites on the adaxial (inner facing) and abaxial (outer facing) surfaces of sepals and petals, and the surfaces of anthers and stigma (Figure 7b).

This imaging technology was used to determine the distribution of individual cuticular lipid metabolites at all four developmental stages of wild-type Arabidopsis flowers, and these images were compared to flowers of the *cer2-5* mutant, and to the *cer2-5* mutant that was transgenically expressing the *Gl2* gene. Figure 7b shows representative data revealing the surface distribution of the most abundant cuticular lipid (C29 alkane), which is evenly distributed on both the adaxial and abaxial floral surfaces of wild-type flowers during the later stages of development (Stages C and D). However,
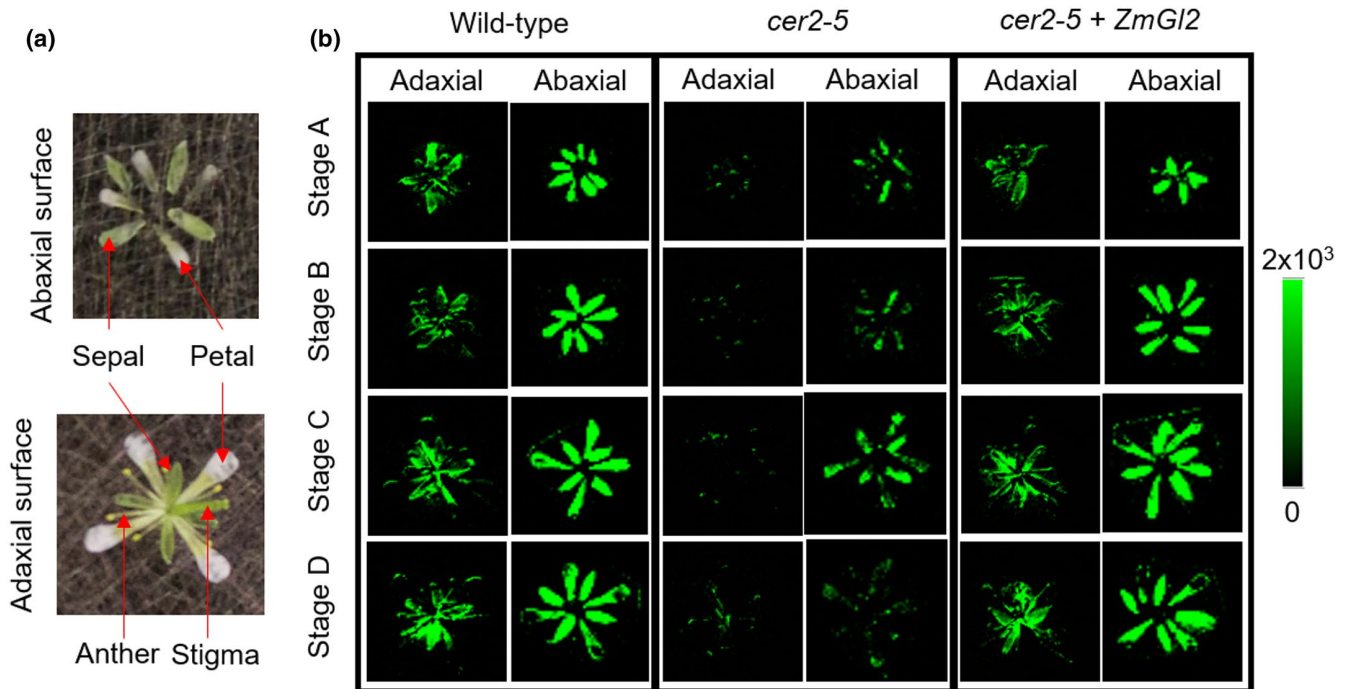
FIGURE 7 Spatial distribution of nonacosane on Arabidopsis flowers. (a) Visual images of the adaxial and abaxial surfaces of Arabidopsis flowers positioned on a MALDI plate ready for mass spectrometric imaging. (b) The distribution of nonacosane (C29 alkane) on the adaxial and abaxial floral surfaces at four stages of development (Stages A to D) of the indicated genotypes. MSI absolute intensity scale bar is color coded: green is maximum signal and black is minimum signal

at the earlier stages of foliar development (Stages A and B), this cuticular lipid is primarily detected on the abaxial surface and occurs at reduced levels on the adaxial surface of the flower (Figure 7b). The *cer2-5* mutation significantly reduced the amount of the C29 alkane on both the adaxial and abaxial floral surfaces, and the transgenic expression of the maize *Gl2* in this mutant background reversed this effect, so that the distribution of this lipid is similar to the distribution found on the wild-type flowers.

Because Stage C flowers display the clearest physical separation of the different flower tissues, MSI analysis was used to evaluate the distribution of a wider range of cuticle metabolites among flower tissues in response to the transgenic expression of *Gl2* and *Gl2-like* in the *cer2-5* mutant background (Figure 8). These imaging experiments specifically focused on the spatial distribution of cuticle metabolites that are metabolically derived from the 30:0 fatty acid, namely C30 aldehyde, and the C29 alkane, secondary alcohol, and ketone. These images reveal that whereas these metabolites are evenly distributed on the abaxial surfaces, they more discreetly localized to the petals, and edges of the sepals of the adaxial surface of wild-type flowers. The *cer2-5* mutant flowers show uniform reduction in the levels of C30 aldehyde, C29 alkane, and C29 ketone on both surfaces of the flower sepals and petals, and the 30:0 fatty acid and the C29 secondary alcohol are at undetectable levels. The transgenic expression of *Gl2* or *Gl2-like* in the *cer2-5* mutant not only increased the levels of these metabolites but also reiterated the distribution patterns of these metabolites to that imaged on the wild-type flowers (Figure 8a,b).

3.4 | MSI can be used to visualize the spatial distribution of individual metabolic conversions of the cuticular biosynthetic network

An additional application of MSI technology is the ability to infer the spatial distribution of the underlying metabolic conversion processes that support a metabolic network. The cuticular lipid metabolic network consists of a series of fatty acyl-CoA elongase reactions that can generate a homologous series of free fatty acids, aldehydes, primary alcohols, alkanes, secondary alcohols, and ketones. Although evidence for all these interconversions have not been directly demonstrated by in vitro enzyme-catalyzed reactions, one can consider duos of these classes of metabolites as potential substrate–product pairs. We illustrate this by the visualization of the colocalization of substrate–product pairs of potential individual metabolic reactions of the cuticular biosynthetic pathway. For example, consider the distribution of pairs of fatty acids, 24:0, 26:0, 28:0, 30:0, and 32:0; each sequential pair has a precursor–product relationship in the reactions of fatty acid elongation. Additionally, each fatty acid has a potential precursor–product relationship with an aldehyde of the same carbon chain length. Figures 9 and 10 and Figures S3 and S4 visualize the spatial distribution of these precursor–product relationships by false color coding of each substrate (green) and each product (red) of these metabolic conversions. In the resulting fused images, the yellow-colored zones indicate the spatial colocation of these precursor–product pairs, indicative of the underlying tissue/cell locations where this metabolic conversion may be occurring.
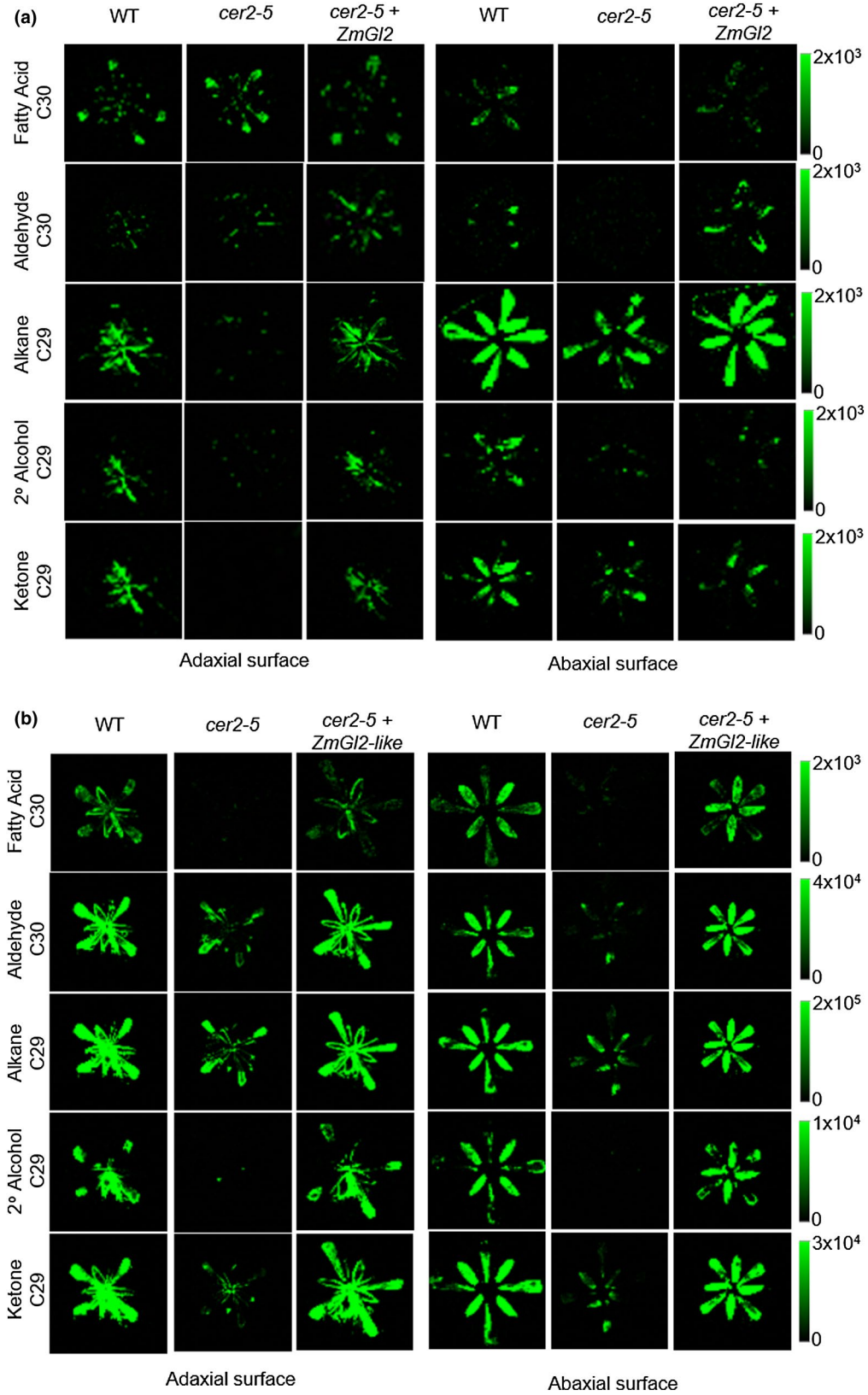
FIGURE 8 Spatial distribution of cuticular lipids on the adaxial and abaxial surfaces of Arabidopsis flowers. Two independent experiments that visualize the effect of the transgenic expression of *Gl2* (a) or *Gl2-like* (b) on the spatial distribution of 30:0 fatty acid and alkyl derivatives on the two surfaces of Arabidopsis flowers. The genotype of each flower is indicated and MSI absolute intensity scale bar is color coded: green is maximum signal and black is minimum signal
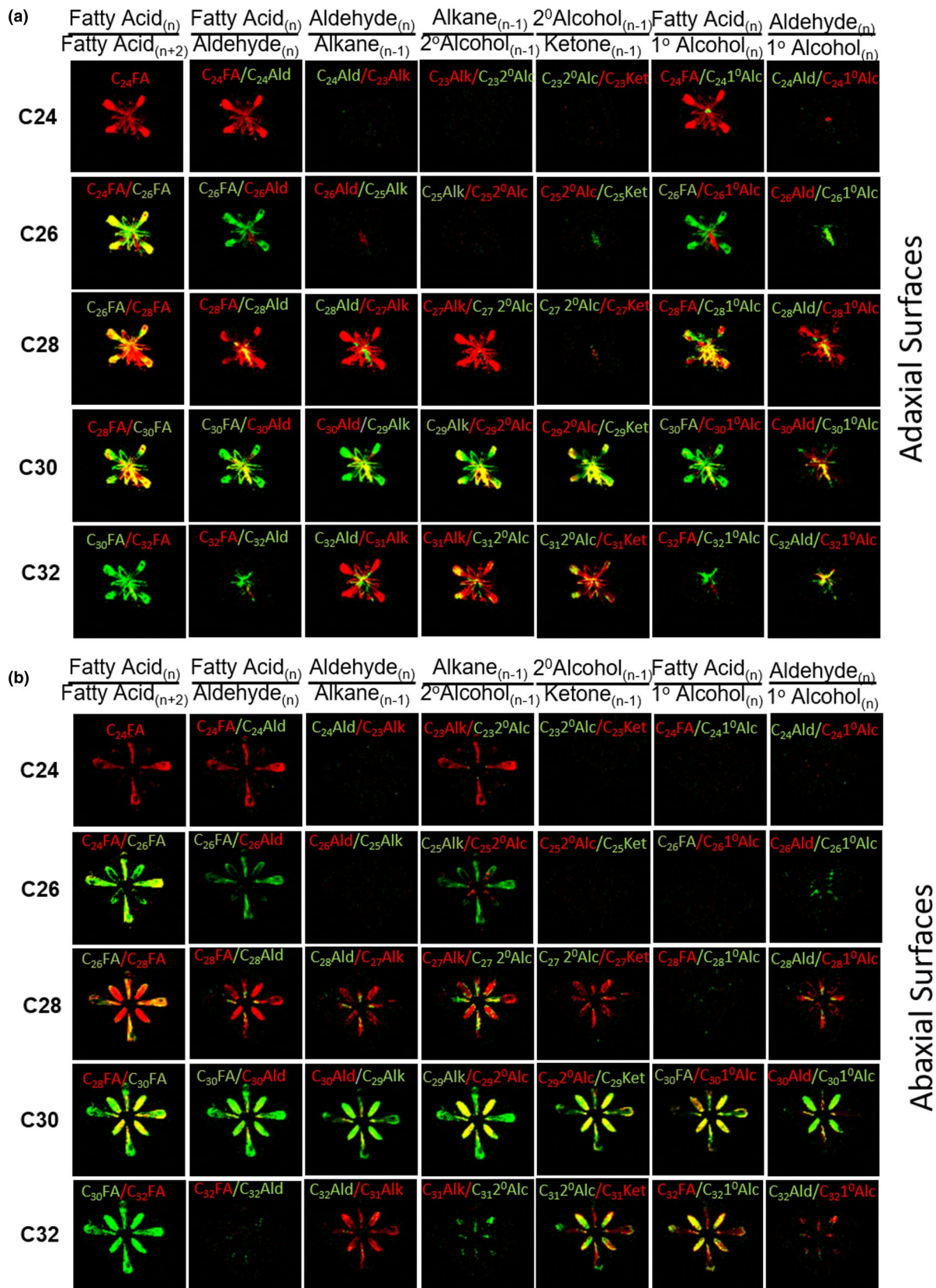
FIGURE 9 Mass spectrometric imaging of the colocalization of substrate–product pairs of individual reactions of the cuticular lipid biosynthesis pathway. Each image is a fusion of two false color-coded MSI images, green for the substrate, and red for the product of a single metabolic reaction that contributes to cuticular lipid biosynthesis pathway. In these fused images, yellow represents the spatial zone where these substrate–product pairs colocalize, indicating the location of the underlying tissue/cells where this metabolic interconversion could be occurring. The distribution of 24:0 to 32:0 fatty acid and their alkyl derivatives on the adaxial (a) and abaxial (b) floral surfaces wild-type Col-0 flowers
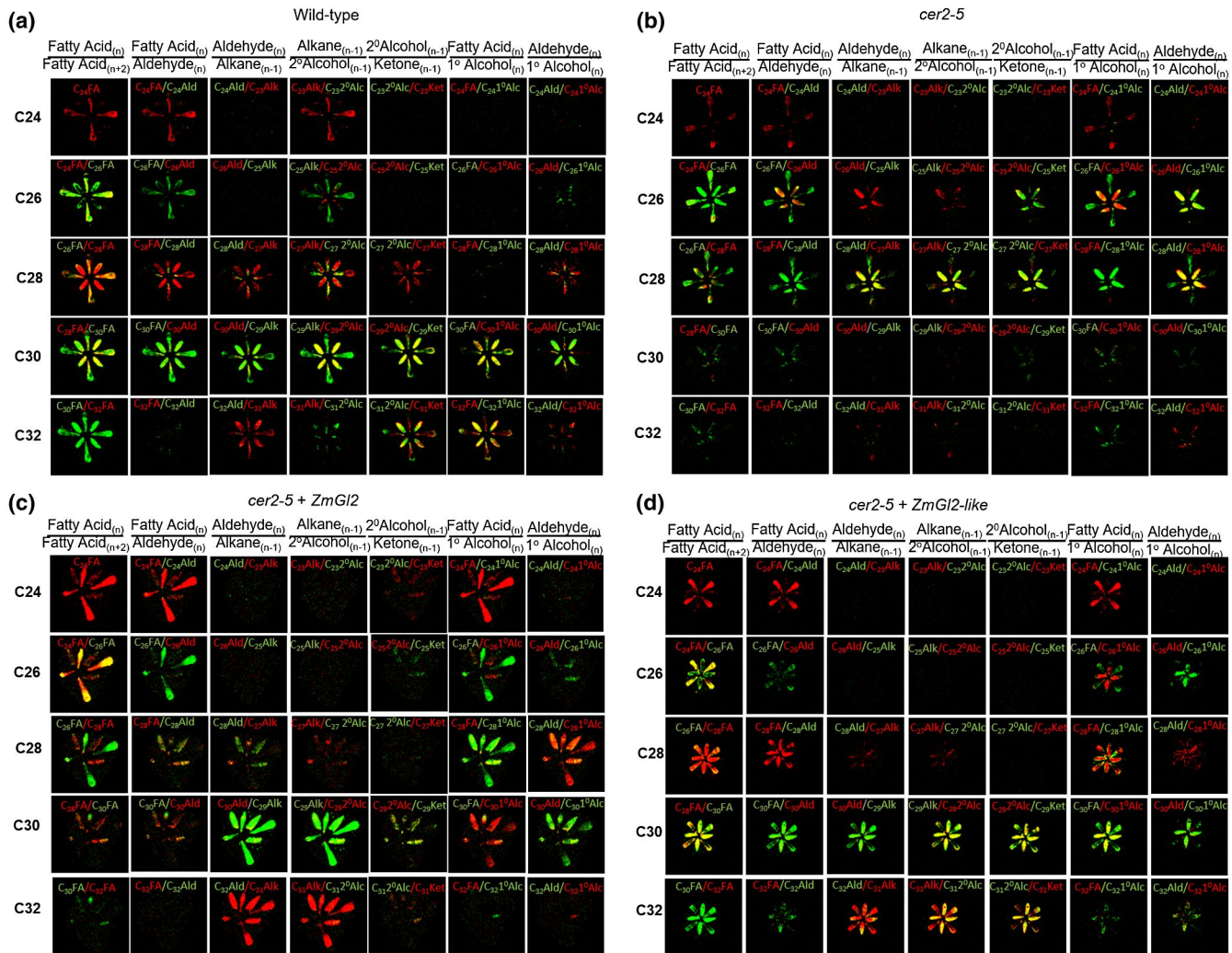
FIGURE 10 Mass spectrometric imaging of the colocalization of substrate–product pairs of individual reactions of the cuticular lipid biosynthesis pathway. Each image is a fusion of two false color-coded MSI images, green for the substrate, and red for the product of a single metabolic reaction that contributes to cuticular lipid biosynthesis pathway. In these fused images, yellow represents the spatial zone where these substrate–product pairs colocalize, indicating the location of the underlying tissue/cells where this metabolic interconversion could be occurring. The distribution of 24:0 to 32:0 fatty acid and their alkyl derivatives on the abaxial floral surfaces are indicated for wild-type Col-0 (a), *cer2* mutant (b), and *cer2* mutant transgenically expressing *Gl2* (c) or *Gl2-like* (d)

Figure 9a shows that the fatty acid precursor–product pairs of the fatty acid elongation reactions predominately colocalize on the adaxial surface of wild-type flower petals. In contrast, there is less such colocalization on the abaxial surface (Figure 9b). Similar colocalization occurs on the adaxial surfaces of the stigmatic tissue and petals (Figure 9a) for the four reactions that lead from 30:0 fatty acid to the C29 ketone (i.e., C_{30} FA-C_{30} Ald, C_{30} Ald-C_{29} Alk, C_{29} Alk-C_{29} 2⁰Alc, and C_{29} 2⁰Alc-C_{29} Ket). And such colocalization is found on the abaxial surface of sepals for the last two reactions of decarbonylative branch (i.e., C_{29} Alk-C_{29} 2⁰Alc and C_{29} 2⁰Alc-C_{29} Ket; Figure 9b). This contrasts with the substrate–product pairs of the reductive branch of the pathway that generates the primary alcohols (i.e., C_{28} FA-C_{28} 1⁰Alc and C_{30} FA-C_{30} 1⁰Alc pairs), these colocalize on the abaxial surface of sepals and stigmatic surfaces (Figure 9).

The *cer2-5* mutation does not affect these colocalization patterns, with the exception of products that are generated from 28:0 and 30:0 fatty acids. Thus, consistent with the proposed role of CER2 in affecting the 28:0 to 30:0 fatty acid elongation process (Hannoufa et al., 1993; Jenks et al., 1995), the 28:0–30:0 fatty acid substrate–product pairs do not colocalize in the *cer2-5* mutant (Figure 10b, Figure S3a). As a result, there are altered spatial accumulation patterns of the C28 alkyl derivatives within both the decarbonylative and reductive branches of the cuticular lipid pathway. Specifically, in the *cer2-5* mutant, the substrate–product pairs from C28 aldehyde to C27 ketone primarily colocalize in the sepals, and the C26 aldehyde–C26 primary alcohol and C28 aldehyde–C28 primary alcohol substrate–product pairs primarily colocalize in the sepals and stigmatic tissue surface. These differential colocalizations in the *cer2-5* mutant may indicate that both the decarbonylative and

reductive branches of the cuticular lipid pathway occur in sepal tissues, but the reductive branch of the pathway appears to predominate in the stigmatic tissues. The transgenic expression of *Gl2-like* in the *cer2-5* mutant background restores the colocalization pattern of the 28:0 and 30:0 fatty acid elongation substrate–product pairs and the decarbonylative and reductive pathway substrate–product pairs to the pattern observed in the wild-type flowers (Figure 10d, Figure S3b). Such a restoration of the substrate–product patterns is also obtained when the *Gl2* is transgenically expressed in the *cer2* mutant (Figure 10c).

These substrate–product colocalization patterns were also identified and compared at different stages of flower development (Figures S4 and S5). These data are presented only for the abaxial surfaces of the flowers because the signal-to-noise ratios obtained from these surfaces were sufficiently high to enable the formulation of robust conclusions (Figure S4), whereas this was not the case for the data gathered from the adaxial surface (Figure S5). During the development of wild-type flowers, the area of colocalization of the fatty acid elongation substrate–product pairs (24:0–28:0) that occurs in the petals decrease as the flowers proceed to Stage D, whereas the colocalization of the 26:0 to 30:0 fatty acid elongation substrate–product pairs becomes concentrated to the sepals (Figure S4). The *cer2-5* mutation disrupts these colocalization patterns, so that throughout flower development only the 24:0–26:0 fatty acid pair colocalize in petals, whereas, the 26:0–28:0 fatty acid pair colocalize to the sepals (Figure S4). The transgenic expression of *Gl2* in the *cer2-5* mutant did not affect these altered colocalization patterns of the 24:0–26:0 fatty acid substrate–product pairs, and no colocalization patterns were observed for the 26:0–28:0 fatty acid pair (Stages C and D; Figure S4).

In wild-type flowers, the spatial pattern of the 28:0–30:0 fatty acid elongation substrate–product pairs is distinct from the substrate–product pairs of the decarbonylative and reductive branches of the pathway that initiate from these two fatty acids. Namely the C28 and C30 aldehydes and alcohols, and the C27- and C29-derived alkanes, ketones, and secondary alcohols colocalize to the abaxial surfaces of sepals, and this pattern is most apparent at the early stages of flower development (Stages A and B; Figure S4). However, later in flower development, these patterns become less colocalized (Stages C and D; Figure S4). In contrast, in the *cer2-5* flowers, these colocalization patterns are altered, particularly for the substrate–product pairs that lead from C25 and C27 alkanes to the analogous ketones, and the substrate–product pairs C26 aldehyde–C26 primary alcohol. Specifically, the sepal colocalization patterns for C25 alkane to C25 ketone pairs are maintained only during the early stages of flower development (Stages A and B; Figure S4), whereas the C27 alkane to C27 ketone pairs, and C26 aldehyde–primary alcohol pair are maintained throughout development (Figure S4). These highlighted *cer2*-dependent alterations in the colocalization of substrate–product pairs are consistent with the proposed role of CER2 in affecting the 28:0 to 30:0 fatty acid conversion resulting in the higher accumulation of precursor fatty acid products, namely 26:0 and 28:0 (Hannoufa et al., 1993;

Haslam et al., 2012; Jenks et al., 1995). The transgenic expression of *Gl2* in the *cer2-5* mutant background restored colocalization of the substrate-product–pairs patterns for the C30 alkyl decarbonylative and reductive pathway on sepals, at least at the early stages of flower development (Stages A and B; Figure S4), but not at the later stages of development (Stages C and D; Figure S4). Therefore, the ability of the *Gl2* transgene to restore the spatial patterns of the C28 and C30 alkyl chain substrate–product pairs to near wild-type patterns, which were disrupted by the *cer2* mutation, further supports recent studies that indicated the functional homology between *Gl2* and *CER2* (Alexander et al., 2020).

4 | DISCUSSION

Elucidating the biochemical mechanisms that regulate the assembly of the plant cuticle is complicated by the multicellular nature of these organisms. This complexity is particularly associated with the fact that the cuticular lipid biosynthetic pathway is restricted to the epidermal cells of aerial plant organs, and the products of this pathway are unidirectionally transported from these cells to the outer surface of plant organs (Jetter et al., 2000; Yeats & Rose, 2008, 2013). Experimental data from molecular genetic characterizations of *gl* and *cer* mutants that affect normal deposition of cuticular lipids are often interpreted relative to a core cuticular lipid biosynthesis pathway, which appear to be common to both maize and Arabidopsis, if not all plants (Bianchi, 1978; Bianchi et al., 1985; Kolattukudy, 1970; Kunst & Samuels, 2009; Lee & Suh, 2013; Post-Beittenmiller, 1996). This pathway integrates fatty acid elongation with either a reductive branch or a decarbonylative branch to generate a diverse set of alkyl lipid products. In this study, we coupled genetic complementation with unique analytical strategies to measure and visualize distinct spatial and temporal patterns of cuticular lipid accumulation within floral tissues during flower development.

4.1 | Dynamics of the distribution of cuticular surface lipids

The majority of past biochemical and molecular studies of the accumulation of cuticular lipids have primarily been limited to a single time point of analysis, overlooking the dynamics of the processes that integrate the developmental program of the tissue/organs that are being evaluated. Furthermore, most such data are collected from the analysis of cuticular lipid extracts prepared from relatively large biological samples that combine lipids generated by a heterogeneous collection of cells and tissues that are most probably of different age and different developmental states. In this study of developing flowers, the application of new, more assiduous analytical technologies provided the platform to address both of these potential limitations to decipher the physiology of cuticular lipid accumulation patterns.

Specifically, we investigated the effect of the *cer2* mutation and the transgenic expression of maize *Gl2* and *Gl2-like* transgenes on

cuticular lipids of Arabidopsis flowers, monitoring the accumulation pattern of these lipids during the course of floral development. Initial characterization of cer2 mutant has been interpreted to indicate that this gene product affects the elongation of fatty acids between 26:0 or 28:0 and 30:0 (Hannoufa et al., 1993; Jenks et al., 1995), a hypothesis that has been further elucidated by partial reconstitution experiments of the fatty acid elongation process in yeast (Haslam et al., 2012, 2015).

In this study, we gathered data with cuticular lipid extracts prepared from individual flowers at four different stages of development. In parallel, we also applied MALDI-MSI to image the spatial distribution of extracellular cuticular lipid metabolites on either the abaxial or adaxial surfaces of the developing flowers at a sufficiently high spatial resolution to distinguish between four different floral organs (petals, sepals, anthers, and stigmatic surfaces) and determined the effect of each genetic manipulation on the extracellular cuticular lipid profiles.

These studies of the dynamics of flower development demonstrate that a block in a metabolic process that specifically occurs in the epidermal cells of the flower tissues (i.e., extracellular cuticular lipid deposition caused by the cer2 mutation) does not affect the developmental timing of the integrated organ, but it does affect the biomass of the flower, particularly when the cer2 mutation is complemented by the two maize homologs. The expression of the maize homologs of CER2, Gl2-like or Gl2 transgenes in the cer2-5 mutant reversed the effect of blocking the accumulation of cuticular lipids on flowers, but these transgenes have differential effects on the growth of the floral organs, where expression of Gl2 reduced the flower biomass, whereas expression of Gl2-like does not alter the flower biomass. These findings indicate, therefore, that the flower biomass trait can be affected by the deposition of the cuticle, possibly associated with the ability of the organ to retain water that is lost via transpiration through a "leaky" cuticle (Goodwin and Jenks, 2005).

During flower development, the majority of the individual cuticular lipid components accumulate at near parallel, asymptotic patterns as the flower developed. The maximum observed rate of cuticular lipid accumulation occurs during the earlier stages of flower development, and this is at a rate of ~26 nmol hr^{-1} g^{-1} fresh weight. This rate defines the minimal rate of de novo fatty acid biosynthesis that is required to feed the FAE system with stearoyl-CoA precursor. Furthermore, because the final products of the cuticular lipid biosynthetic pathway are components that are predominantly derivatives of 30-carbon fatty acids, six elongation cycles of the FAE system are required to elongate the 18:0 fatty acyl-CoA precursor to these final products. Because each elongation cycle requires one molecule of malonyl-CoA generated from the cytosolic acetyl-CoA pool, and two molecules of NADPH, one can infer the minimal rates of acetyl-CoA (156 nmol hr^{-1} g^{-1} fresh weight) and NADPH (312 nmol hr^{-1} g^{-1} fresh weight) generation in the cytosol that is required to support the observed rate of cuticle lipid deposition. Prior characterizations of ATP-citrate lyase (Fatland et al., 2002, 2005) and the cytosolic homomeric acetyl-CoA carboxylase (Baud et al., 2003; Konishi & Sasaki, 1994;

Yanai et al., 1995), which sequentially generate the cytosolic acetyl-CoA and malonyl-CoA pools, appear to indicate that there is sufficient activity of these enzymes in Arabidopsis tissue to provide this rate of acetyl-CoA and malonyl-CoA generation. Similarly, there appears to be sufficient activities of NADPH-generating enzymes (NADP+-dependent malic enzyme, glucose-6-phosphate dehydrogenase, and 6-phosphogluconate dehydrogenase) to support these needs of the FAE system (Wakao et al., 2008; Wakao & Benning, 2005; Wheeler et al., 2005; Yin and Ashihara, 2008).

These rates can be compared to experimentally determined rates of de novo fatty acid biosynthesis of ~0.3–0.6 μmol hr^{-1} mg^{-1} of chlorophyll by isolated chloroplasts (Gardiner et al., 1984) or intact leaves (Browse et al., 1981; Murphy & Leech, 1981). Although it is difficult to make a direct comparison between our determined rates and these earlier determined rates, assuming that the chlorophyll concentration of leaf tissue is ~1.2 mg/g fresh weight (e.g., Jin et al., 2011), one can deduce that only a small portion of tissue fatty acid biosynthetic capability is destined to support cuticle deposition. Moreover, a more recent study found that the rate of cuticle deposition by isolated stem epidermal tissue was ~1 μg/hr/cm^2 stem area (Suh et al., 2005). Making the assumptions that these cuticular lipids are predominantly of 30-carbon fatty acid derivatives (i.e., molecular weight ~450 Da), and that Arabidopsis stems have a diameter of ~2 mm and a tissue density of 1 g/cm^3, one can calculate that this reported rate is equivalent to ~40 nmol hr^{-1} g^{-1} fresh weight, which compares with our experimentally determined rate of ~26 nmol hr^{-1} g^{-1} fresh weight of flower tissue.

The effect of the cer2-5 mutation is to reduce the rate of cuticular lipid accumulation at the early stages of flower development by about 55% (to ~12 nmol hr^{-1} g^{-1} fresh weight), and this rate plateaus to near zero later in flower development. As expected, the transgenic expression of CER2 in the cer2-5 mutant background reverses the initial rate of cuticular lipid accumulation to that of wild-type state, enabling the normal levels of cuticular lipid accumulation. Similarly, the transgenic expression of Gl2 (but not Gl2-like) also reverses the effect of the cer2 mutation, increasing the rate of cuticular lipid accumulation to that of wild-type levels. In contrast, Gl2-like transgene increases the rate of cuticular lipid accumulation, but does not fully restore this rate to the wild-type level.

In all these genetically complemented lines, the near asymptotic pattern of cuticular lipid accumulation is shared by nearly all individual cuticular lipid components, and the rates of accumulation are higher than in the cer2-5 mutant. The exception to this generalization is the accumulation pattern displayed by the primary alcohols and fatty acids, particularly of 26- and 28-carbon chain length, which increase in accumulation in the cer2-5 mutant as compared to the wild-type flowers. The transgenic expression of Gl2 or Gl2-like in the cer2-5 mutant reverses these alterations in the accumulation of C26 and C28 primary alcohols and fatty acids (i.e., reduces accumulation) to the wild-type state. In combination, these genetic complementation experiments reinforce the conclusion that two maize genes have overlapping functionalities that are homologous to the CER2 gene function (Alexander et al., 2020). Furthermore, these

data may suggest the existence of two parallel fatty acid elongation processes, one feeding the decarbonylative branch of the pathway and the other feeding the reductive branch. Thus, the *CER2* gene may affect the fatty acid elongation processes that feed the decarbonylative branch, and when this is blocked by the *cer2* mutation, fatty acyl-CoA intermediates are diverted to the fatty acid elongation processes that feed the reductive branch, leading to increased primary alcohols.

4.2 | High spatial resolution dynamics of cuticular surface lipids

The larger accumulation of cuticular lipids on the abaxial side of the flower, primarily localized to the sepals, is consistent with the function of the cuticle as a water barrier (Aarts et al., 1995; Jung et al., 2006; Millar et al., 1999). Namely, because the sepals enclose the flower bud, their abaxial surfaces are outward facing, and thus the larger cuticular lipid load would provide more extensive protection from the desiccating environment.

Flowers transgenically expressing the *Gl2* or *Gl2-like* transgenes proved useful in visualizing the spatial distribution of the cuticular lipid biosynthetic reactions. This was accomplished by the colocalizing spectral images of substrate–product pairs of specific reactions of different segments of the cuticular lipid pathway. Thus, MSI analysis of flowers transgenically expressing the maize *Gl2* or *Gl2-like* genes demonstrates that the core processes of fatty acid elongation occur predominantly in the petals of flowers. Subsequently, the products of the FAE system are processed through the decarbonylative or reductive branch of the pathway. The colocalization spectral images of substrate–product pairs indicate that the decarbonylative branch is primarily expressed in the stigmatic tissue and sepals, and the reductive branch of the pathway is primarily expressed in the stigmatic tissue.

Therefore, the data presented in this study revealed previously unknown attributes concerning the spatial and temporal changes in cuticular lipid accumulation patterns, as affected by different genotypes and by flower development. These were revealed by the application of novel analytic technologies that directly assessed the accumulation of the metabolic intermediates and products of this complex pathway. Previously, these were inferred by assessing cell-specific expression of genes and proteins associated with this pathway (Greer et al., 2007; Kim et al., 2019; Xia et al., 1996), using indirect measurements of gene expression (e.g., fluorescent markers or in situ hybridization). Although these analyses provide valuable insights on the gene expression program(s) that regulate cuticular lipid deposition, it is difficult to dissect how these networks are regulated if one does not also have insights on the spatial and temporal patterns of the metabolic intermediates and products of the pathway. Moreover, because this pathway is expressed by a single cell layer, it is also important to evaluate the heterogeneous spatial distribution of the products of the pathway across plant surfaces. In this study this heterogeneity was revealed relative to the different flower organs (i.e., sepals, petal, stigma, and styles) and in relation to the abaxial and adaxial surfaces of these organs. Therefore, the metabolite imaging technique, coupled with specialized gas chromatography inlet that was used herein, has proven to be a powerful combination for detecting the differential distribution and developmental changes in cuticular lipid deposition, providing new insights on the temporo-spatial granularity of the pathway. The application of these new analytical technologies has provided new insights into the cuticular lipid biosynthesis pathway. These include: (a) a quantitative measure of the minimum flux through the pathway; (b) the finding that the reductive and decarbonylative branches of the pathway are spatially sequestered into separate flower organs; (c) the functional homology between the Arabidopsis *CER2* gene and the maize *Gl2* and *Gl2-like* genes; and (d) that the *cer2* mutation differentially affects the reductive and decarbonylative branches of the pathway on the pistil (i.e., stigma and style) and the perianth (i.e., petal and sepal) organs of the flower, respectively. Hence, these new insights reveal complexities in the spatiotemporal accumulation patterns of the products of this pathway that will need more detailed biochemical and molecular dissection in order to mechanistically understand how the cuticular lipid biosynthesis pathway is regulated.

AUTHOR CONTRIBUTIONS

B.J.N. conceived the project; L.E.A. generated and characterized transgenic lines, performed the single-flower gas-chromatography experiments, and analyzed the data; B.X., L.E.A., and J.G. performed mass spectral imaging and data analysis and Z.S provided technical support in many aspects of the research; J.G. was an undergraduate research assistant supported by the SULI program of the Department of Energy Ames Laboratory; and all authors contributed to the writing of the article.

ORCID

Liza E. Alexander https://orcid.org/0000-0002-5244-8259
Basil J. Nikolau https://orcid.org/0000-0002-4672-7139

REFERENCES

Aarts, M. G., Keijzer, C. J., Stiekema, W. J., & Pereira, A. (1995). Molecular characterization of the CER1 gene of arabidopsis involved in epicuticular wax biosynthesis and pollen fertility. *The Plant Cell, 7*, 2115–2127. https://doi.org/10.1105/tpc.7.12.2115

Alexander, L. E., Okazaki, Y., Schelling, M. A., Davis, A., Zheng, X., Rizhsky, L., Yandeau-Nelson, M. D., Saito, K., & Nikolau, B. J. (2020). Maize Glossy2 and Glossy2-like genes have overlapping and distinct functions in cuticular lipid deposition. *Plant Physiology*. *183*, 840 LP–853. https://doi.org/10.1104/pp.20.00241

Alvarez-Buylla, E. R., Benítez, M., Corvera-Poiré, A., Chaos Cador, Á., de Folter, S., Gamboa de Buen, A., Garay-Arroyo, A., García-Ponce, B., Jaimes-Miranda, F., Pérez-Ruiz, R. V., Piñeyro-Nelson, A., & Sánchez-Corrales, Y. E. (2010). Flower development. *The Arabidopsis Book*, *8*, 1–57. https://doi.org/10.1199/tab.0127

Amstalden van Hove, E. R., Smith, D. F., Fornai, L., Glunde, K., & Heeren, R. M. A. (2011). An alternative paper based tissue washing method for mass spectrometry imaging: localized washing and fragile tissue analysis. *Journal of the American Society for Mass Spectrometry*, *22*, 1885–1890. https://doi.org/10.1007/s13361-011-0203-z

Angel, P. M., & Caprioli, R. M. (2013). Matrix-assisted laser desorption ionization imaging mass spectrometry. *Situ Molecular Mapping. Biochemistry*, *52*, https://doi.org/10.1021/bi301519p

Baud, S., Guyon, V., Kronenberger, J., Wuillème, S., Miquel, M., Caboche, M., Lepiniec, L., & Rochat, C. (2003). Multifunctional acetyl-CoA carboxylase 1 is essential for very long chain fatty acid elongation and embryo development in Arabidopsis. *The Plant Journal*, *33*, 75–86. https://doi.org/10.1046/j.1365-313x.2003.016010.x

Bernard, A., & Joubès, J. (2013). Arabidopsis cuticular waxes: Advances in synthesis, export and regulation. *Progress in Lipid Research*, *52*, 110–129. https://doi.org/10.1016/j.plipres.2012.10.002

Bianchi. (1975). Glossy mutants of maize. VI. Chemical constituents of glossy-2 epicuticular waxes. *Maydica*, *20*, 165–173.

Bianchi, A. (1978). Glossy mutants: Level of action and level of analysis. In *Maize breeding and genetics* (pp. 533–550). John Wiley and Sons.

Bianchi, A., Bianchi, G., Avato, P., & Salamini, F. (1985). Biosynthetic pathways of epicuticular wax of maize as assessed by mutation, light, plant age and inhibitor studies. Maydica (Italy).

Browse, J., Roughan, P. G., & Slack, C. R. (1981). Light control of fatty acid synthesis and diurnal fluctuations of fatty acid composition in leaves. *The Biochemical Journal*, *196*, 347–354. https://doi.org/10.1042/bj1960347

Cha, S., Song, Z., Nikolau, B. J., & Yeung, E. S. (2009). Direct profiling and imaging of epicuticular waxes on arabidopsis thaliana by laser desorption / ionization mass spectrometry using silver colloid as a matrix. *Analytical Chemistry*, *81*, 2991–3000. https://doi.org/10.1021/ac802615r

Chalfie, M., Tu, Y., Euskirchen, G., Ward, W. W., & Prasher, D. C. (1994). Green fluorescent protein as a marker for gene expression. *Science*, *263*(5148), 802–805. https://doi.org/10.1126/science.8303295

Cookson, S. J., Radziejwoski, A., & Granier, C. (2006). Cell and leaf size plasticity in Arabidopsis: What is the role of endoreduplication? *Plant, Cell and Environment*, *29*, 1273–1283. https://doi.org/10.1111/j.1365-3040.2006.01506.x

D'Auria, J. C. (2006). Acyltransferases in plants: A good time to be BAHD. *Current Opinion in Plant Biology*, *9*, 331–340. https://doi.org/10.1016/j.pbi.2006.03.016

Dong, Y., Li, B., & Aharoni, A. (2016). More than pictures: When MS imaging meets histology. *Trends in Plant Science*, *21*, 686–698.

Engewald, W., Teske, J., & Efer, J. (1999). Programmed temperature vaporisers-based large volume injection in capillary gas chromatography. *Journal of Chromatography A*, *842*, 143–161. https://doi.org/10.1016/S0021-9673(99)00080-1

Fatland, B. L., Ke, J., Anderson, M. D., Mentzen, W. I., Cui, L. W., Allred, C. C., Johnston, J. L., Nikolau, B. J., & Wurtele, E. S. (2002). Molecular characterization of a heteromeric ATP-citrate lyase that generates cytosolic acetyl-coenzyme A in Arabidopsis. *Plant Physiology*, *130*, 740–756.

Fatland, B. L., Nikolau, B. J., & Wurtele, E. S. (2005). Reverse genetic characterization of cytosolic acetyl-CoA generation by ATP-citrate lyase in Arabidopsis. *The Plant Cell*, *17*, 182–203.

Feenstra, A. D., Alexander, L. E., Song, Z., Korte, A. R., Yandeau-Nelson, M. D., Nikolau, B. J., & Lee, Y. J. (2017). Spatial mapping and profiling of metabolite distributions during germination. *Plant Physiology*, *174*, https://doi.org/10.1104/pp.17.00652

Gallagher, S. R. (1992). *GUS protocols: Using the GUS gene as a reporter of gene expression*. Academic Press.

Gardiner, S. E., Heinz, E., & Roughan, P. G. (1984). Rates and products of long-chain Fatty Acid synthesis from [1-^{14}C]acetate in chloroplasts isolated from leaves of 16:3 and 18:3 plants. *Plant Physiology*, *74*, 890–896.

Goodwin, S. M., & Jenks, M. A. (2005). Plant cuticle function as a barrier to water loss. In M. A. Jenks, & P. M. Hasegawa (Eds.), *Plant abiotic stress*. Oxford.

Greer, S., Wen, M., Bird, D., Wu, X., Samuels, L., Kunst, L., & Jetter, R. (2007). The cytochrome P450 enzyme CYP96A15 Is the midchain alkane hydroxylase responsible for formation of secondary alcohols and ketones in stem cuticular wax of arabidopsis. *Plant Physiology*, *145*(3), 653–667. https://doi.org/10.1104/pp.107.107300

Griffin, B. A., Adams, S. R., & Tsien, R. Y. (1998). Specific covalent labeling of recombinant protein molecules inside live cells. *Science*, *281*(5374), 269–272. https://doi.org/10.1126/science.281.5374.269

Hannoufa, A., McNevin, J., & Lemieux, B. (1993). Epicuticular waxes of eceriferum mutants of Arabidopsis thaliana. *Phytochemistry*, *33*, 851–855. https://doi.org/10.1016/0031-9422(93)85289-4

Haslam, T. M., Gerelle, W. K., Graham, S. W., & Kunst, L. (2017) The unique role of the ECERIFERUM2-LIKE clade of the BAHD acyltransferase superfamily in cuticular wax metabolism. *Plants (Basel)*, *6*, 23.

Haslam, T. M., Haslam, R., Thoraval, D., Pascal, S., Delude, C., Domergue, F., Fernandez, A. M., Beaudoin, F., Napier, J. A., Kunst, L., & Joubes, J. (2015). ECERIFERUM2-LIKE proteins have unique biochemical and physiological functions in very-long-chain fatty acid elongation. *Plant Physiology*, *167*, 682–692. https://doi.org/10.1104/pp.114.253195

Haslam, T. M., Mañas-Fernández, A., Zhao, L., & Kunst, L. (2012). Arabidopsis ECERIFERUM2 is a component of the fatty acid elongation machinery required for fatty acid extension to exceptional lengths. *Plant Physiology*, *160*, 1164–1174. https://doi.org/10.1104/pp.112.201640

Jellings, A. J., & Leech, R. M. (1982). The importance of quantitative anatomy in the interpretation of whole leaf biochemistry in species of triticum, hordeum and avena. *New Phytologist*, *92*, 39–48. https://doi.org/10.1111/j.1469-8137.1982.tb03361.x

Jenks, M. A., Tuttle, H. A., Eigenbrode, S. D., & Feldmann, K. A. (1995). Leaf epicuticular waxes of the eceriferum mutants in arabidopsis. *Plant Physiology*, *108*, 369–377. https://doi.org/10.1104/pp.108.1.369

Jetter, R., Schäffer, S., & Riederer, M. (2000). Leaf cuticular waxes are arranged in chemically and mechanically distinct layers: Evidence from Prunus laurocerasus L. *Plant, Cell & Environment*, *23*, 619–628.

Jin, B., Wang, L., Wang, J., Jiang, K. Z., Wang, Y., Jiang, X. X., Ni, C. Y., Wang, Y. L., & Teng, N. J. (2011). The effect of experimental warming on leaf functional traits, leaf structure and leaf biochemistry in Arabidopsis thaliana. *BMC Plant Biology*, *11*, 35. https://doi.org/10.1186/1471-2229-11-35

Jun, J. H., Song, Z., Liu, Z., Nikolau, B. J., Yeung, E. S., & Lee, Y. J. (2010). High-spatial and high-mass resolution imaging of surface metabolites of arabidopsis thaliana by laser desorption-ionization mass spectrometry using colloidal silver. *Analytical Chemistry*, *82*, 3255–3265. https://doi.org/10.1021/ac902990p

Jung, K.-H., Han, M.-J., Lee, D., Lee, Y.-S., Schreiber, L., Franke, R., Faust, A., Yephremov, A., Saedler, H., Kim, Y.-W., Hwang, I., & An, G. (2006). Wax-deficient anther1 Is Involved in Cuticle and Wax Production in Rice Anther Walls and Is Required for Pollen Development. *The Plant Cell*, *18*, 3015 LP–3032. https://doi.org/10.1105/tpc.106.042044

Jungmann, J. H., & Heeren, R. M. A. (2012). Emerging technologies in mass spectrometry imaging. *Journal of Proteomics*, *75*, 5077–5092. https://doi.org/10.1016/j.jprot.2012.03.022

ALEXANDER ET AL.

17 of 18

American Society
of Plant Biologists

SEB SOCIETY FOR EXPERIMENTAL BIOLOGY

WILEY

Kaspar, S., Peukert, M., Svatos, A., Matros, A., & Mock, H. P. (2011). MALDI-imaging mass spectrometry – An emerging technique in plant biology. *Proteomics*, 11, 1840–1850.

Kheibarshekan Asl, L., Dhondt, S., Boudolf, V., Beemster, G. T. S., Beeckman, T., Inzé, D., Govaerts, W., & De Veylder, L. (2011). Model-based analysis of arabidopsis leaf epidermal cells reveals distinct division and expansion patterns for pavement and guard cells. *Plant Physiology*, 156(4), 2172–2183. https://doi.org/10.1104/pp.111.181180

Kim, H., Yu, S.-I., Jung, S. H., Lee, B. H., & Suh, M. C. (2019). The F-Box protein SAGL1 and ECERIFERUM3 regulate cuticular wax biosynthesis in response to changes in humidity in Arabidopsis. *The Plant Cell*, 31(9), 2223–2240. https://doi.org/10.1105/tpc.19.00152

Kolattukudy, P. E. (1970). Biosynthesis of cuticular lipids. *Annual Review of Plant Physiology*, 21, 163–192. https://doi.org/10.1146/annurev.pp.21.060170.001115

Konishi, T., & Sasaki, Y. (1994). Compartmentalization of two forms of acetyl-CoA carboxylase in plants and the origin of their tolerance toward herbicides. *Proceedings of the National Academy of Sciences United States of America*, 91, 3598–3601. https://doi.org/10.1073/pnas.91.9.3598

Koo, J., Kim, Y., Kim, J., Yeom, M., Lee, I. C., & Nam, H. G. (2007). A GUS/luciferase fusion reporter for plant gene trapping and for assay of promoter activity with luciferin-dependent control of the reporter protein stability. *Plant & Cell Physiology*, 48, 1121–1131.

Koornneef, M., Hanhart, C. J., & Thiel, F. (1989). A Genetic and phenotypic description of eceriferum (cer) mutants in Arabidopsis thaliana. *Journal of Heredity*, 80, 118–122. https://doi.org/10.1093/oxfordjournals.jhered.a110808

Kunst, L., & Samuels, L. (2009). Plant cuticles shine: Advances in wax biosynthesis and export. *Current Opinion in Plant Biology*, 12, 721–727. https://doi.org/10.1016/j.pbi.2009.09.009

Küpper, H., Seib, L. O., Sivaguru, M., Hoekenga, O. A., & Kochian, L. V. (2007). A method for cellular localization of gene expression via quantitative in situ hybridization in plants: Quantitative in situ hybridization. *The Plant Journal*, 50, 159–187. https://doi.org/10.1111/j.1365-313X.2007.03031.x

Lee, S. B., & Suh, M. C. (2013). Recent advances in cuticular wax biosynthesis and its regulation in arabidopsis. *Mol. Plant*, 6, 246–249. https://doi.org/10.1093/mp/sss159

Lee, Y. J., Perdian, D. C., Song, Z., Yeung, E. S., & Nikolau, B. J. (2012). Use of mass spectrometry for imaging metabolites in plants. *The Plant Journal*, 70, 81–95. https://doi.org/10.1111/j.1365-313X.2012.04899.x

Leide, J., Hildebrandt, U., Reussing, K., Riederer, M., & Vogg, G. (2007). The developmental pattern of tomato fruit wax accumulation and its impact on cuticular transpiration barrier properties: Effects of a deficiency in a beta-ketoacyl-coenzyme A synthase (LeCER6). *Plant Physiology*, 144, 1667–1679.

McDonnell, L. A., & Heeren, R. M. A. (2007). Imaging mass spectrometry. *Mass Spectrometry Reviews*, 26, 606–643. https://doi.org/10.1002/mas.20124

McFadden, G. I. (1995). Chapter 12 in situ hybridization. *Methods in Molecular Biology*, 49, 165–183. https://doi.org/10.1016/S0091-679X(08)61453-3

McNevin, J. P., Woodward, W., Hannoufa, A., Feldmann, K. A., & Lemieux, B. (1993). Isolation and characterization of eceriferum (cer) mutants induced by T-DNA insertions in Arabidopsis thaliana. *Genome/National Research Council Canada = Genome/Conseil National De Recherches Canada*, 36, 610–618.

Millar, A. A., Clemens, S., Zachgo, S., Giblin, E. M., Taylor, D. C., & Kunst, L. (1999). CUT1, an arabidopsis gene required for cuticular wax biosynthesis and pollen fertility, encodes a very-long-chain fatty acid condensing enzyme. *The Plant Cell*, 11, 825 LP–838. https://doi.org/10.1105/tpc.11.5.825

Murphy, D. J., & Leech, R. M. (1981). Photosynthesis of lipids from CO_2 in Spinacia oleracea. *Plant Physiology*, 68, 762–765.

Negruk, V., Yang, P., Subramanian, M., McNevin, J. P., & Lemieux, B. (1996). Molecular cloning and characterization of the CER2 gene of Arabidopsis thaliana. *The Plant Journal*, 9, 137–145. https://doi.org/10.1046/j.1365-313x.1996.09020137.x

Ow, D. W., De Wet, J. R., Helinski, D. R., Howell, S. H., Wood, K. V., & Deluca, M. (1986). Transient and stable expression of the firefly luciferase gene in plant cells and transgenic plants. *Science*, 234, 856. https://doi.org/10.1126/science.234.4778.856

Pascal, S., Bernard, A., Sorel, M., Pervent, M., Vile, D., Haslam, R. P., Napier, J. A., Lessire, R., Domergue, F., & Joubes, J. (2013). The Arabidopsis cer26 mutant, like the cer2 mutant, is specifically affected in the very long chain fatty acid elongation process. *The Plant Journal*, 73, 733–746.

Post-Beittenmiller, D. (1996). Biochemistry and Molecular Biology of Wax Production in Plants. *Annual Review of Plant Physiology and Plant Molecular Biology*, 47, 405–430. https://doi.org/10.1146/annurev.arplant.47.1.405

Robinson, D. O., Coate, J. E., Singh, A., Hong, L., Bush, M., Doyle, J. J., & Roeder, A. H. K. (2018). Ploidy and size at multiple scales in the arabidopsis sepal. *The Plant Cell*, 30(10), 2308–2329. https://doi.org/10.1105/tpc.18.00344

Samuels, L., Kunst, L., & Jetter, R. (2008). Sealing plant surfaces: Cuticular wax formation by epidermal cells. *Annual Review of Plant Biology*, 59, 683–707. https://doi.org/10.1146/annurev.arplant.59.103006.093219

Schnable, P. S., Stinard, P. S., Wen, T.-J., Heinen, S., Weber, D., Zhang, L., Hansen, J. D., & Nikolau, B. J. (1994). The genetics of cuticular wax biosynthesis. *Maydica*, 39, 279–287.

Smyth, D. R., Bowman, J. L., & Meyerowitz, E. M. (1990). Early flower development in arabidopsis. *The Plant Cell*, 2, 755–767. https://doi.org/10.1105/tpc.2.8.755

Suh, M. C., Samuels, A. L., Jetter, R., Kunst, L., Pollard, M., Ohlrogge, J., & Beisson, F. (2005). Cuticular lipid composition, surface structure, and gene expression in Arabidopsis stem epidermis. *Plant Physiology*, 139, 1649–1665. https://doi.org/10.1104/pp.105.070805

Svatoš, A. (2010). Mass spectrometric imaging of small molecules. *Trends in Biotechnology*, 28, 425–434. https://doi.org/10.1016/j.tibtech.2010.05.005

Tacke, E., Korfhage, C., Michel, D., Maddaloni, M., Motto, M., Lanzini, S., Salamini, F., & Doring, H. P. (1995). Transposon tagging of the maize Glossy2 locus with the transposable element En/Spm. *The Plant Journal*, 8, 907–917.

Vogg, G., Fischer, S., Leide, J., Emmanuel, E., Jetter, R., Levy, A. A., & Riederer, M. (2004). Tomato fruit cuticular waxes and their effects on transpiration barrier properties: Functional characterization of a mutant deficient in a very-long-chain fatty acid beta-ketoacyl-CoA synthase. *Journal of Experimental Botany*, 55, 1401–1410.

Wakao, S., Andre, C., & Benning, C. (2008). Functional analyses of cytosolic glucose-6-phosphate dehydrogenases and their contribution to seed oil accumulation in Arabidopsis. *Plant Physiology*, 146, 277–288.

Wakao, S., & Benning, C. (2005). Genome-wide analysis of glucose-6-phosphate dehydrogenases in Arabidopsis. *The Plant Journal*, 41, 243–256.

Wang, X., Guan, Y., Zhang, D., Dong, X., Tian, L., & Qu, L. Q. (2017). A β-ketoacyl-CoA synthase is involved in rice leaf cuticular wax synthesis and requires a CER2-LIKE protein as a cofactor. *Plant Physiology*. 173, 944 LP–955. https://doi.org/10.1104/pp.16.01527

Wheeler, M. C. G., Tronconi, M. A., MaF, D., Andreo, C. S., Flügge, U.-I., & VnG, M. (2005). A comprehensive analysis of the NADP-malic enzyme gene family of Arabidopsis. *Plant Physiology*, 139, 39–51.

Wilson, B., Wylie, P. L., & Klee, M. S. (1997). *Large-volume injection for gas chromatography using a PTV Inlet; Application Note 5965-7770E.* Agilent Technology.

Wilson, B., Wylie, P. L., & Klee, M. S. (2000). Large Volume Injection for Gas Chromatography Using a PTV Inlet I, 1–6.

Xia, Y., Nikolau, B. J., & Schnable, P. S. (1996). Cloning and characterization of CER2, an Arabidopsis gene that affects cuticular wax accumulation. *The Plant Cell*, *8*, 1291–1304. https://doi.org/10.1105/tpc.8.8.1291

Yanai, Y., Kawasaki, T., Shimada, H., Wurtele, E. S., Nikolau, B. J., & Ichikawa, N. (1995). Genomic organization of 251 kDa acetyl-CoA carboxylase genes in Arabidopsis: Tandem gene duplication has made two differentially expressed isozymes. *Plant & Cell Physiol.*, *36*, 779–787. https://doi.org/10.1093/oxfordjournals.pcp.a078822

Yeats, T. H., & Rose, J. K. (2008). The biochemistry and biology of extracellular plant lipid-transfer proteins (LTPs). *Protein Science*, *17*, 191–198. https://doi.org/10.1110/ps.073300108

Yeats, T. H., & Rose, J. K. (2013). The formation and function of plant cuticles. *Plant Physiology*, *163*, 5–20. https://doi.org/10.1104/pp.113.222737

Yin, Y., & Ashihar, H. (2008). Expression of glucose-6-phosphate dehydrogenase and 6-phosphogluconate dehydrogenase isoform genes in suspension-cultured Arabidopsis thaliana cells. *Zeitschrift Für Naturforschung C*, *63*, 713–720.

Yu, D., Ranathunge, K., Huang, H., Pei, Z., Franke, R., Schreiber, L., & He, C. (2008). Wax Crystal-Sparse Leaf1 encodes a β–ketoacyl CoA synthase involved in biosynthesis of cuticular waxes on rice leaf. *Planta*, *228*, 675–685. https://doi.org/10.1007/s00425-008-0770-9

SUPPORTING INFORMATION

Additional Supporting Information may be found online in the Supporting Information section.